Article Citation Format
Ibrahim M. A. & Adigun A. A. (2019): Development of Local Feature Models for Accurate Detection and Classification of Medical Images. Journal of Advances in Mathematical & Computational Sciences Vol. 7, No. 4. Pp 9-22

Article Progression Time Stamps

Article Type: Research Article
Manuscript Received 11th November, 2019
Final Acceptance: 17th December, 2019
Article DOI: dx.doi.org/10.22624/AIMS/MATHS/V7N4P2

Development of Local Feature Models for Accurate Detection and Classification of Medical Images

[1]Ibrahim M. A. &[2] Adigun A. A.
Department of Information and Communication Technology
Osun State University, Osogbo, Nigeria
E-mail: [1]ibrahima@uniosun.edu.ng, [2]fempej2013@gmail.com
Phone: +2348134249446; +2348033749081

ABSTRACT

The effectiveness of local or global features has recently attracted growing attention in the field of texture image classification and retrieval. The features of the local binary pattern (LBP) for instance, usually lack global spatial information while global descriptors would provide very little local information. This paper proposes two different descriptors to circumvent these shortcomings by providing more information to describe different textural structures of the Emphysema computed tomography (CT) images. The proposed LBP+Multi- fractal Images (LMI) and the rotational invariant LBP+Multi- fractal Images (RLMI) can provide more accurate classification results by using a hybrid concatenation of the local and global features. The experimental approaches are validated for different scales of Emphysema images during the classification process in order to determine the appropriate image size that could yield the maximum classification accuracy. The experimental results show that the descriptors extracted from the combined features considerably improve the performance of the classifiers. The results also indicate that the LMI descriptor outperforms the earlier approaches and demonstrate the discriminating power and robustness of the combined features for accurate classification of Emphysema CT images.

Keywords: Texture, classification; multi-fractal images; emphysema images; feature selection; histogram

1. INTRODUCTION

Texture analysis has been widely applied in different areas of image processing and computer vision. These applications include image retrieval, object identification, medical image analysis and image segmentation. Local binary pattern (LBP) is a simple but effective way of characterizing the local intensity distribution of an image. Multi-resolution LBP or combinations of different LBPs descriptors and variants have demonstrated to be more effective in texture image analysis than ordinary LBP. However, since the LBP uses only the local characteristics of the image, this sometime limits the accuracy and the overall performances, especially when dealing with a high dimensional feature space [1].

Local histogram computation of digital images is a very powerful discriminating tool as it gives useful information that could be used in texture classification, retrieval and segmentation problems [2][3][4]. The LBP descriptors could be implemented in the form of a rotation - invariant feature of the intensity values or without rotation [5], [6][7]. It has recently proven to be a very powerful tool in the field of texture image classification and retrieval. Verma and Zisserman [8] recently developed a model for scale invariant texture classification where the histogram of texton based dictionary is used as a descriptor. Some recent works have been done that reported texture classification using the fractal analysis [9], which also achieved great success. In [10], the author compares a center symmetric pair of pixels to construct LBP labels. Additionally, the author in [3] combines the features from the normal LBP operator with the patterns from the local intensity differences and center pixel gray level. The effectiveness of the multi- fractal spectrum to classify the structure of different bread types in digital images were recently investigated [11].

The authors used different fractal features of the image for the classification of bread crumb types with high accuracy. A new texture descriptor was developed by combining the information from the spatial domain with the frequency domains [9], this is achieved by robustly encoding the multi-scale information of the textures; the proposed texture descriptor is very robust to scale and rotation changes. Furthermore, in [12], different rotation invariant features are extracted from histograms of local non invariant patterns to construct a new descriptor, which is an effective descriptor for dynamic recognition. But despite these great successes that have been achieved by the LBP-based approaches in the texture classification, face recognition and analysis, it poses some challenges since it only gives the local properties of the object. Reference [13] proposed two different fusion approaches by combining different LBP variants with the same radius and number of neighbourhoods as descriptors.

The patterns are extracted in different forms using the Fourier transform to generate different descriptors to train a set of support vector machine (SVM). The research showed that the combination of LBP and its variant always outperform the individual descriptors, a good example is demonstrated by [5], [6] where a joint histogram of LBP and its variant outperformed each individual descriptor [14]. Reference [1] proposed a data mining approach to extract the patterns from the computation of local binary codes and variants of LBP with multiple radii. The author uses the combination of the feature selection techniques to select the best set of features with the high discriminative ability on the training images. The research also indicates that each of the LBP variants has its advantages and disadvantages; combining complementary variants may further improve their capability, but the challenge is the selection of the proper LBP features and how they are combined [1]. Since the traditional LBP has these shortcomings such as, lacking of global information and

sensitivity to noise [15], this study therefore proposed the development of a new descriptor by combining the local information from the LBP-based approach with the global features from the multi-fractal features in order to reduce some of the limitations of ordinary LBP. The proposed method could use the information from the local and global features to classify different textural structures of the images. First and foremost, ordinary LBP would be calculated by comparing the centre pixels of each image with its neighbouring pixels to generate the LBP codes[14][16]. General comparative analyses could also be accomplished using some performance measures like the classification accuracy, time complexity, processor memory usage and so on between the multi-fractal methods (a- image and $f(\alpha)$ image) and the LBP. We also propose to combine the LBP histogram features derived from the efficient LBP features with the features generated from the multi-fractal approach to generate a new descriptor that could be used for the classification process.

The performances of the new descriptors obtained after the normalization and feature selection are investigated, would be compared with the results obtained in the recently published paper by [17], which uses the joint LBP for the classification of Emhysema images. The experimental analysis would be investigated using different image sizes in order to see the effects on the performances and how it relates to the associated parameters. The second approach would combine the feature vectors derived from both rotation invariant local binary pattern (RILBP) histogram and the alpha image features to construct another descriptor for the classification and analysis of Emphysema images. The reason for concatenating the LBP-based features with the multi-fractal features is that, this idea would provide a generalization of the local intensity distributions and eventually gives the global characterizations of the images.

This proposed idea tends to compensate the global features or characteristics that the LBP is lacking since the multi-fractal feature is known as a global descriptor of digital images as discussed in these articles [18]– [20]. The combined features approach would hopefully provide a powerful tool that could be used for efficient texture classification. The feature selection could be used to select the highly discriminating features that could yield better results and reduce the space and time complexities. The rest of the paper is organized as follows: In section 2, the LBP and its variants are reviewed, sections 3 and 4 discuss the proposed methods and the feature selection technique, in sections 5 and 6, experimental analyses and results are presented, and finally, section 7 summarizes the results and gives some feature research directions.

2. LOCAL BINARY PATTERNS

The Local Binary Pattern (LBP) operator can be defined according to [14] as a texture operator that labels the pixels of an image by thresholding the neighbourhood of each pixel and considers the results as binary numbers. The gray scale variance of the neighbourhood, is specified using P sampling points on a circle of radius R as in (1).

$$LBP_{P,R} = \Sigma_{p=0}^{P-1} s(g_p - g_c)2^p \quad (1)$$

$$s(x) = \begin{cases} 1, \text{ if } x \leq 0; \\ 0, \text{ otherwise} \end{cases} \quad (2)$$

where gc is the gray value at the central pixel, gp is the value of its neighbours, P is the total number of involved neighbours, and R is the radius of the neighbourhood. LBP is uniform if the binary pattern contains at most two bitwise transitions from 0 to 1 or vice versa when the bit pattern is traversed circularly. A uniform pattern can be applied to reduce the length of the feature vector and implement a simple rotation-invariant descriptor. The example showing in Fig.1 illustrates the normal calculation of the LBP from the intensity values of the Emphysema image pixels where the threshold value is 38 and after comparison with the neighbourhood values, the corresponding LBP binary codes are generated. Similarly, in Fig. 2, we have shown how the structural patterns of the image change with the efficient LBP codes and the RILBP after applying the radial filter. It is noted from the structure of the images that efficient LBP is darker than the corresponding rotation invariant; this is expected because the magnitude of the intensity values of the image pixels in the efficient LBP is higher than the equivalent pixel values in the RILBP. Though, they both receive the same binary codes when converted using the LBP approach; that is, LBP: 11111111 and RILBP: 11111111.

The magnitude of the centre pixels (Threshold) within the normal image is 38, which is higher than the corresponding pixels in efficient LBP and RILBP since the 2D radial filter has removed some unwanted information that may be present within the image. These changes in the center pixels also demonstrate that the LBP is sensitive to noise and it also illustrates how important the center pixel is in texture characterization. The centre pixels also describe the gray level of the local patch and contain additional discriminant information that might be very useful during the classification process. The corresponding histograms for the regular LBP and the RILBP are shown with the images as presented in Fig. 2. There is an option to extract two different features from the RILBP, that is, the rotation invariance sparse histogram and the rotation invariance tight-histograms as presented in Fig. 2.

3. PATTERN AND FEATURE SELECTION

Feature selection is the process of identifying and eliminating the irrelevant and redundant features from the data set in order to reduce the dimensionality of the data and allow the learning algorithms to operate faster as the model complexity reduces. This can sometimes increase the classification accuracy and facilitate easy interpretation of the models. One of the approaches to dimensionality reductions is to transform a high dimensional feature space into a lower dimensional space [21][22] as this reduces the model complexities. In [16], the linear discriminant analysis (LDA) is combined with the principal component analysis (PCA) to obtain high discriminative patterns from a high dimensional feature space derived from the descriptors.

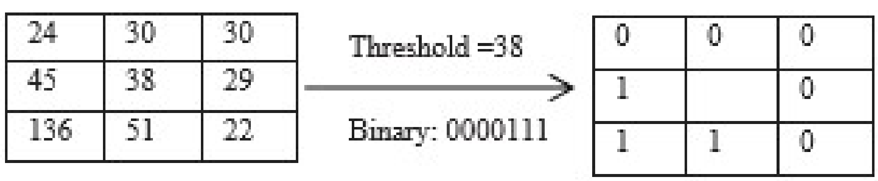

Figure 1: Illustrating the example of LBP code of an Emphysema image

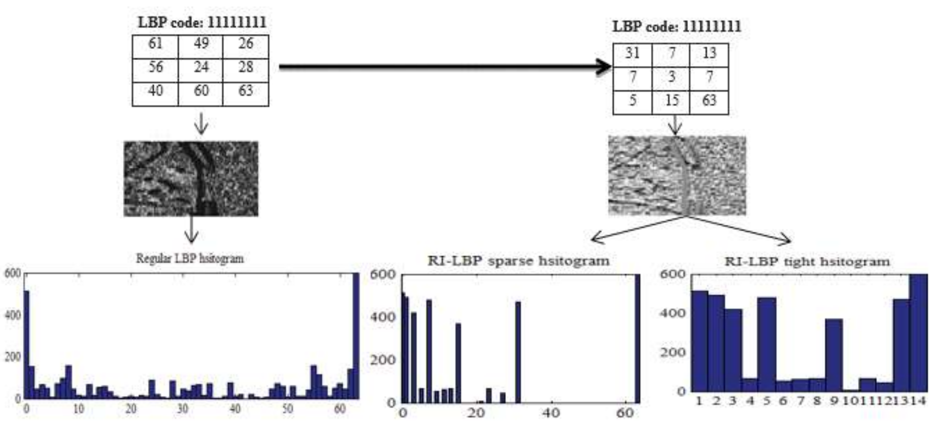

Figure 2: Illustrating different structural patterns of LBP and their corresponding codes

The authors later applied Laplacian PCA (LPCA) to maximize the weighted local scatter instead of the global scatter of data as in the original PCA [16]. The results achieved significantly improved the classification accuracy. In this research, in order to select the most highly discriminating features from the LBP-based feature vectors and the multi-fractal features, we propose to calculate the column area under the curve (AUC) of all the features extracted and find the maximum mean AUC values for the best four columns in each data set. The four columns with the highest average AUC values would be selected as a four dimensional feature vector space for each data set during the classification process.

4. METHODS

The system overview of the construction of feature vectors that uses the LBP-based approach combined with the multi- fractal methods to generate a new descriptor LMI is given in Fig. 3. The input image from the Emphysema database is filtered by using the radial filter function generated from the MATLAB. A round or radial filter is a 2D matrix generated using a specifying number of neighbours, which represents a different number of enabled filter elements and the radius of the filter. A circular filter is generated by subtracting the grey values of the centre pixel from the neighbouring pixels at different rotation angles as provided by [5]. The efficient LBP is obtained by the general approach of comparing the centre pixel to the neighbouring ones. In this implementation, a general radial filter is introduced to get rid of the unwanted features such that only the useful information could be used for the computation of LBP, the illustration on the effectiveness of this approach is demonstrated in Fig. 3.

The rotation invariant descriptor is obtained using a search for the appropriate angle at which the LBP value of a given pixel is minimal; the angle of rotation and the numbers of neighbours are other useful parameters that may influence the performances of the RILBP features. The RILBP histogram would always use less bins than the regular LBP since it induces an effective means of calculating the number of bins. In RILBP, the angle of rotation can be improved by the number of neighbouring points or the radius of the pixels. The RILBP would only concentrate on the relevant values by assigning a weight vector to the neighbouring pixels surrounding the unique pixels at the centre. Various invariants could also be attained by shifting or rotating in such a way that the minimum possible values for a unique RILBP could be accomplished. A tight histogram of the LBP is generated by changing the input matrix or image contrast, such that the bins are uniformly arranged or distributed and no empty bins exists within the histogram. This is accomplished by using a flag to determine if the histogram is tight (no empty bins) or if the minimum and maximum values of the input image are uniformly distributed.

5. EXPERIMENTAL ANALYSIS

In this study, different experimental approaches are conducted on the features extracted from the Emphysema patches using the LBP and f(α) image feature vectors computed. The details of the computation of the multi-fractal parameters like the alpha images, f(α) images and fractal dimensions of digital images can be found in the previous studies [18]–[20],[23]. The original size of the patches of the Emphysema database is 61*61 pixels, but all the patches were rescaled into different window sizes in order to investigate different scale invariants for the classification accuracies.

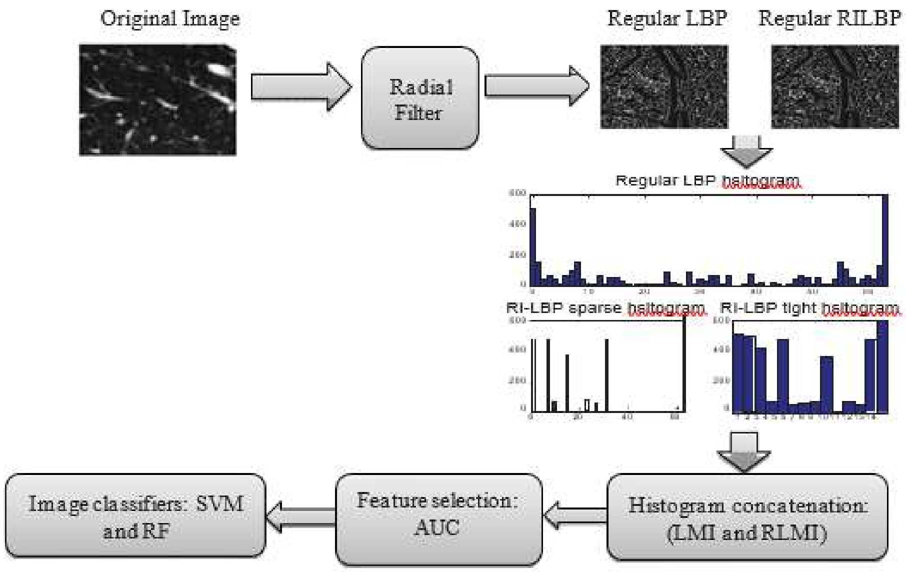

Figure 3. System overview of the Emphysema classification using the LMI and RLMI descriptors

The classification system is tested with the patches of different sizes: 64*64, 128*128, 256*256, 320*320, 384*384 and 512*512 pixels. The features extracted from the efficient LBP are the corresponding pixel values obtained from the LBP histogram calculated after filtering with the radial filter and adjusted the bin size of the histogram into an appropriate size. The multi-fractal features are derived from the computation of fractal dimension of the corresponding pixels in the Emphysema image patches. In this research, we considered three different types of Emphysema patches, the Normal tissue (NT) Emphysema, centrilobular Emphysema (CLE) and Paraseptal Emphysema (PSE) using different window sizes of the corresponding patches. 50 images were selected from each Emphysema class and the intensity values of the calculated LBP histogram and the $f(\alpha)$ image features for each patch are arranged in rows towards the corresponding class labels to generate the data set, this is repeated for the 50 images in each group making up a total of 150 images.

After the pixel arrangements, in both LBP and $f(\alpha)$ image, we obtained a total of 9600*64, 19200*128, 38400*256, 48000*320, 57600*384 and 76800*512 pixels for 150 images in each NT,CLE and PSE Emphysema images respectively. The corresponding pixels obtained from the two descriptors are concatenated as proposed to generate a new descriptor LMI, which is utilized in the classification procedures. The total data sets obtained after the concatenation are 9600*128, 19200*256, 38400*512, 48000*640, 57600*768 and 76800*1024 for the 64*64, 128*128, 256*256, 320*320, 384*384 and 512*512 patches respectively. The same procedure is repeated for the construction of the second descriptor where the alpha image features obtained from the multi-fractal based technique is also concatenated with the RILBP features as proposed. The dimensions of the images for both features remain the same as described and the newly constructed feature descriptor (RLMI) is also used in the classification process. During this process, the feature vector of each data set is clustered using 3 clusters in order to view how the data set are grouping.

Fig. 4 presents how the intensity distributions of a 64*64 window size image after clustering are grouped. Another exploratory test that could be useful would be to determine the correlation within the feature vectors in order to determine how correlated or uncorrelated the feature variables within the data sets are? As can be seen in Fig. 4, the k-means clustering was able to group together those features with similar attributes into the same category. The second class CLE, has the highest number and it is indicated by the red colour, followed by the NT in black colour at the middle and lastly the PSE group with the green colour. This approach would help us to understand the general arrangement or an overview of the data sets before the classification process. As previously stated, these features are the combined features originally extracted from the efficient LBP histograms and the $f(\alpha)$ image feature vectors (joint histogram concatenation).

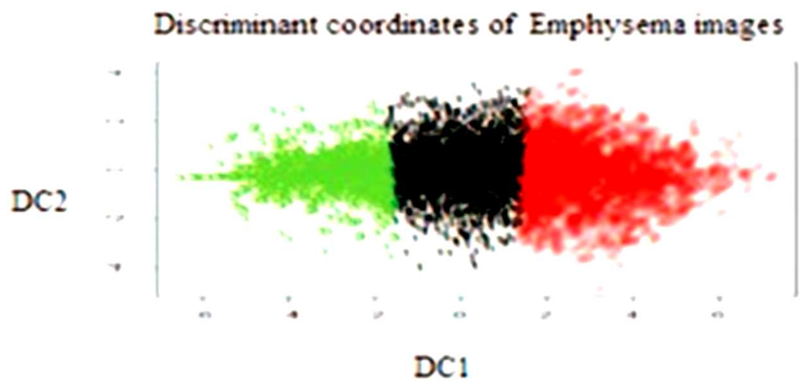

Figure 4. Illustrating the grouping of the Emphysema classes after clustering

The matrix dimension after this concatenation process for a 64*64 pixel size is 19200*128, which is of course a high dimensional data set. After determining the correlation between the feature vectors, it was discovered that there are many irrelevant and redundant features that are not useful, which could be eliminated. The column AUC is calculated to extract the feature variables with the important information that could be used to improve the classification accuracy. This is done for each data set and the four columns with the highest average AUC values are chosen for further classification process, while the observations or the matrix rows remain unchanged. We could as well use the PCA for the feature selection or sequential feature selection techniques. For further understanding and the analysis of the data sets, Fig. 5 presents the receiver operating characteristic (ROC) curves of the feature vector with the maximum AUC values (best features) for the patches with the window sizes of 64*64, 128*128 and 256*256.

The corresponding class pairwise AUC for each curve in the three data sets with different window sizes, is calculated and the results are shown in Fig. 5. The results in Fig. 5 indicate that the data sets with the highest window size (256*256) give the best total AUC value (0.6668), followed by the data sets with 128*128 pixel size, which also give a total AUC value of 0.6544. Lastly, the features with the smallest patch size has the lowest AUC value as it can be seen from the corresponding ROC curves presented in Fig. 5. This process has really helped to simplify the models in each data by reducing the matrix dimension from 128columns for a 64*64 pixel image, 256columns for a 128*128 pixel image and lastly 512columns for a 256*256 pixel image into just four columns.

This process of dimensionality reduction would definitely reduce the time and space complexities during the classification process and probably increase the classification accuracy as complex models sometimes over fit data sets and hence introduces errors. The simplified model would not only appropriately fit the data, but also save the memory utilization and the processor execution time. According to the system overview shown in Fig. 3, we propose to normalize the histogram data before applying the classifiers for the data classification. Another way to determine the differences within the data group is by using the multiple comparisons. The Tukey's test [24] is employed in this research to check further how significantly different are those groups within the data sets. Then a multiple comparison could be used to search for the specific differences between the possible pairwise groups in the data sets.

After applying the Tukey Pairwise comparisons on the data sets for the grouping information, the results after the test assign letter 'a' to CLE, letter 'b' to NT and letter 'c' to PSE, which indicates they do not share a letter, that is, the classes are significantly different. The information provided in the data sets could also be used to check which pair of means is significantly different, and which are not using the multiple comparisons. Multiple comparisons could also be used to display a graph with each class mean represented by a symbol and an interval around the symbol. Two means are said to be significantly different if their means are disjointed, but insignificantly different if their intervals overlap. In Table 1, it can be observed that the mean values of the pairwise class in the NT and CLE classes are significantly different from other classes, which is in line with the ROC curves generated in Fig. 5 which shows that it is easier to separate NT-CLE pairwise classes from others than the CLE-PSE and NT-PSE pairwise classes.

The estimated values of the means for other class pairs are not significantly separated from each other as NT-CLE class does, which indicates that it is really difficult to separate these pairwise classes from each other and other classes. This is also demonstrated in Fig. 5 using the ROC curves. The NT versus CLE indicated with blue colour in the ROC curves in Fig. 5 is clearly separated from other classes while the CLE versus PSE and NT versus PSE pairwise classes are very close to each other and even the estimated values of the means in the Table 1 also confirm this with a p-value <0.0001 and about 95% confidence interval. This is enough evidence for us to confirm how the data sets are grouped using the information provided. The details of the framework for the concatenation approach for the development of the two descriptors used in the experimental analysis are shown in Fig. 6. The original Emphysema images are rescaled into different scale invariances for the joint combination of the features.

In Fig. 6, different features are extracted from the original Emphysema images using the multi-fractal decomposition and the LBP-based approaches, the features are jointly combined in the form of hybrid to generate a histogram descriptor, which is used for the classification tasks using different image classifiers. That is, the $f(\alpha)$ and LBP features are mapped together to form a descriptor while the RILBP and the a-image features are mapped together to generate the second descriptor for the experimental analyses.

6. CLASSIFICATION APPROACH AND ANALYSIS

In order to evaluate the discriminating capability of the combined features from the two descriptors, different classification experiments are conducted. Three Emphysema classes are defined with 50 images, assigned to each class. A comparison is made between the LMI descriptor and the result obtained from the recently published journal. We employ two different image classifiers due to the nature of the datasets used in this study; the SVM, and random forests (RF)[25]. The RF could be a perfect classifier for the multi-fractal datasets since it is relatively robust to outliers and noise, and always enhance better accuracy when random features are used.

The RF randomly selects inputs or a combination of inputs to grow each tree. This can significantly improve the classification accuracy by combining trees grown using random features, and the generalization error of the forests reduces as the number of trees becomes large[25]. SVMs have demonstrated highly competitive performance in many real-world applications, such as bioinformatics, face recognition and image processing [26]– [28]. In [26], SVM outperformed most of the previously proposed methods in the diagnosis of cancer microarray data. Lining and Lipo [29] designed a biased maximum margin analysis and semi-supervised biased maximum margin analysis combined with the SVM to improve the performance of the traditional SVM as a relevance feedback for content based image retrieval (CBIR). In [30], a novel algorithm for subspace learning technique was developed using SVM to exploit the user historical feedback log data for a CBIR. Approximately 70% of the entire data set is used to train different SVM classifiers and 30% of the data sets generated are used for the testing. The results indicate that the LMI presents good classification performance, particularly with the RF classifier, though; the results obtained from the SVM are also good for the LMI. It is noted from the results that the effects of the window size on the data sets are very obvious.

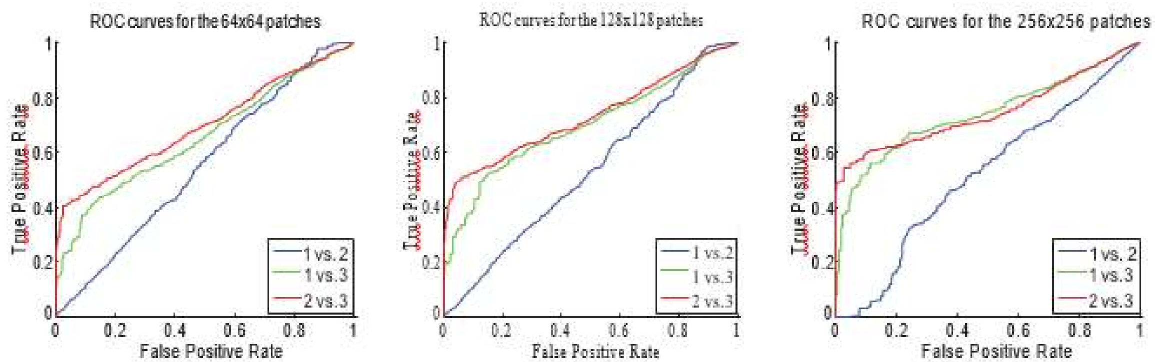

Figure 5. ROC curves for the best features selected from each data set of the three possible pairwise class combinations

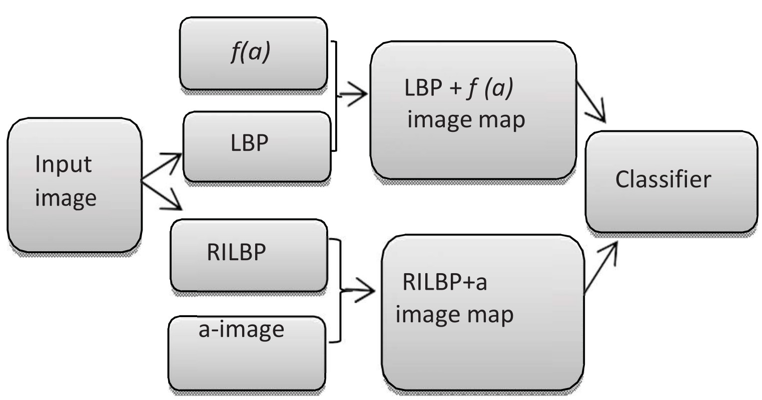

Figure 6. Overview of the joint concatenation methods for the development of the descriptors

Table 1: Multiple Comparisons of Means Using The Tukey's Test

Multiple comparisons of Emphysema class				
P. group	***mean values***	***Std. error***	***t-values***	***P values***
NT-CLE	0.025306	0.005119	4.944	P<0.0001
PSE-CLE	0.233890	0.005119	45.693	P<0.0001
PSE-NT	0.208585	0.005118	40.753	P<0.0001

In Table 2, we can see that, as the image resolution increases, the classification accuracy also increases. In other words, the data sets with the largest image sizes gave the best classification accuracy, using two different classifiers while the data sets with the smallest image pixel size gave the lowest performance. These results also show that as the image size is increasing the overall classification accuracy is also increasing, which indicates that the larger the window size, the higher the classification accuracy. This is simply because the images with the larger sizes have captured more useful information, which eventually increase the discriminating power of the features used in the classification process. The original size of the patches does not contain enough discriminative information, which led to the reduction in the performance accuracy of the classification system. Overall, the performance of the LMI descriptor looks very good as the classification accuracy falls within the range of 75.1-99%.

The scale invariance in the Emphysema images has really influenced the performance of the classification system, though, 512*512 resolution size is the maximum that we have tested with this descriptor. The performance of the classification system that uses 512*512 pixels has been impressive with an accuracy of 99%, even with big data sets, which are about 76800*1024 pixels after the concatenation. Probably, a further increase in the image window sizes might produce worse or better classification accuracy, but of course a classification accuracy of 99% is an excellent result. Generally, the RF classifier performed better than the SVM in all the cases, since the classification accuracy of the SVM classifier falls within the range of 50–62%. The scale invariance approach slightly affects the performances of the SVM classifier, but it is not as prominent as it does in the RF approach. The poor performances of the SVM classifier might be because it has not been trained with enough data sets, reducing the testing sets and increasing the training sets could probably increase the performances of the classifiers. The second descriptor that uses the combined features from the RILBP and the a-images would be experimentally analyzed with the same procedures as the LMI. The classification results of the RILMI descriptor using different image sizes with two different image classifiers are presented in Table 3.

Table 2: Classification Results Of The Lbp-F(A) Descriptor

Classification accuracy – LBP- *f(a)*		
Image Sizes	***SVM***	***RandomForest***
64 * 64	52.08%	75.16%
128 * 128	55.06%	82.58%
256 * 256	61.73%	94.85%
320 * 320	60.1%	97.15%
384 * 384	62%	98.15
512 * 512	60%	99%

Table 3. Classification Results of the Rilbp-Alpha Descriptor

Classification accuracy – RILBP- α		
Image Sizes	***SVM***	***RandomForest***
64 * 64	48.99%	57.46%
128 * 128	48.81%	46.91%
256 * 256	49.89%	47.25%

Performances of the RILMI descriptor are generally lower than the results we have obtained from the LMI. Similarly, the scale invariance of different patch sizes does not have any significant impact on the classification accuracy. However, in the LMI descriptor, the effect of the window sizes of the patches is very obvious, this is expected because the data sets from the RILBP do not really require further invariance examination as this has been done during implementation. Overall, the results are not really bad, but the LMI outperforms the classification results obtained from the RILMI descriptor. Since the changes in the scale invariance to the corresponding results of the classification are not so obvious, the maximum image size tested during the experiment is therefore 256*256. The features derived from the LMI descriptor have higher discriminative power than the features obtained from the RLMI. The next stage of the experimental analysis compares the results obtained from the LMI descriptor with the classification results obtained in the recently published articles [17].

The confusion matrix with the best classification accuracy, which uses the LMI descriptor with the image size of 512*512 pixels, is presented in Table 4 for comparison with the recently published paper, the state-of-art methods for the Emphysema classification. As can be seen in Table 4, our results compare favourably with the LBP results; the overall accuracy of 99% from the confusion matrix obtained from the Emphysema image analysis compared to the accuracy of 95.2% that was achieved showed that the performance of the proposed descriptor is better in spite of a large volume of data sets. Additionally, our approach is simpler and faster in terms of time complexity. It has been verified experimentally that the execution run time to generate the $f(\alpha)$ features is about 5 times faster than the time it would take to calculate LBP features using the same image size. Take for instance, for a 128*128 pixel size, the regular LBP run time was around 3.8s whereas it took just 0.7s to generate the $f(\alpha)$ image of the same image size. Similarly, for a 512 * 512, the execution run time for the regular LBP was around 53.14s while both a and $f(\alpha)$ features can be calculated in just 9.9s.

The experimental tests for the time complexities were carried out for four different image sizes; that is; 64*64, 128*128, 256*256 and 512*512 for comparison between the regular LBP and the $f(\alpha)$ image features. Generally, the LBP consumes more computational time than the $f(\alpha)$ image. This can be very important, especially when dealing with a very large volumeof data sets like 512*512 during classifications, which are around 76800*1024 pixels. The details of the computational time for both feature descriptors are presented in Table 5 using different image patches. The framework of this study provided solutions to few research questions in the field of image classifications. For instance, how does the feature extracted from the combination of LBP and multi-fractal descriptors behave under the same scale changes? Which of these features is dominant over the other? How does the descriptor generally compare with the related previous work using other textural classification approaches?

It has been demonstrated in this research work the effectiveness of the combined features derived from both LBP and the multi-fractal descriptors in the classification of the Emphysema images. In the experimental analysis, we could see how powerful this descriptor is and how it behaves under different scale changes. Although, the multi-fractal features; that is the $f(\alpha)$ and the a-image features have shown to be more powerful or more discriminating than the other features from the LBP and RILBP as this was verified during the experiments. This explains the importance of global features obtained from the multi-fractal descriptors $f(\alpha)$ compared to the local features from the LBP and the combined features from both descriptors, which also behave well under different scale changes.

Some of the important parameters that are very useful during the experimental analysis for the RF classifier are the number of growing trees and the number of the predictor variables. Though, since most data sets used in the experiments are high dimensional data, the Column AUC is applied to reduce the dimension of the data sets into just four predictor variables. It was confirmed during the experimental analyses that as the number of growing trees increases for constructing the classification models, the classification accuracy also increases. This process is used to determine the appropriate number of growing trees that could yield the best classification accuracy.

Table 4: Comparison of Classification Results Using the New Descriptor and The LBP Approach

		LBP			LBP-f(α)		
Actual		***Predicted***			***Predicted***		
		NT	CLE	PSE	NT	CLE	PSE
	NT	93	0	7	99	0	1
	CLE	2	98	0	1	99	0
	PSE	3	2	95	1	0	99

Table 5: Computational Time Comparisons Between The Multi- Fractal Falpha Image And The Regular LBP

Computational Time in seconds		
Image size	***Falpha image***	***Regular LBP***
64 *64	0.3217s	1.3431s
128 *128	0.7173s	3.804s
256 * 256	2.3865s	13.8164s
512 * 512	9.9017s	53.1436s

7. CONCLUSION AND FUTURE WORK

In this study, we have analyzed the effect of different scale invariants on the Emphysema image classification using two different descriptors. We have shown that the proposed descriptors could perform well even with big data sets, especially the LMI that has really shown excellent performances in all cases. This is a great achievement as the classification of large data sets involved in this experiment may sometimes pose some challenges that may affect the performances of the classification system. But, in this case, as the data sets increases, the classification accuracy increases until the algorithm converges. The two descriptors proposed; the LMI and the RILMI were defined to extract the textural characteristics of the images combined with the global properties for the classification of the images.

We have also demonstrated using the LMI that the window sizes of the image have great influence on the classification accuracy. The combined feature that uses the LMI is better than the other descriptor (RILMI). Likewise, the fusing of the LBP and $f(\alpha)$ either in a joint or hybrid form produced a very good performance with overall classification accuracy of 99%. LMI also outperforms the results obtained from the recently published article by [17], which demonstrated the effectiveness and robustness of the proposed descriptor. The classification result that uses the original image scale (64*64) from the Emphysema database indicate that, the LMI achieves 75.16% using the RF classifier while the RILMI reaches only 52.08%. This demonstrates that even before applying the scale invariances, LMI outperforms the RILMI descriptors, which shows that the features from LMI possess better discriminating power than the features from RILMI. Additionally, the scale invariance changes in patches do not have any significant changes in the classification accuracy in the RILMI descriptor, but in the LMI, an increase in the scale of the patches further increases the classification accuracy.

This proves that the changes in the scale invariance of the Emphysema patches further increase the discriminating capability of the features in the LMI descriptor. This is an indication that the features extracted from the LMI cope well with the scale changes, but the features from the RLMI did not really do well with the scale changes in the image patches. Also, the performance of the RF classifier outperforms the SVM in all cases, though this improvement is not much in the RILMI since the classification accuracy has a range of 40-60%, but this improvement can be seen in the LMI as the accuracy increases from 50-60% in SVM to 75-99% in RF under different scale changes. One of the limitations in this research framework is that the RILMI features did not combine well with the alpha image features and that can be seen in the performances of the descriptor during the classification process.

Also in LMI, an increase in the data sets keeps increasing the classification accuracy, but also demanding more memory usage and the processor computational time. In order to improve the performances of the RILMI descriptor, changes in the parameters like the number of neighbours, radius of pixels and even the angle of rotating the LBP when calculating the RILBP might provide better results. The column AUC for the feature selection and high dimensional reduction worked really well, but the PCA for a dimensional reduction might yield better results.

REFERENCES

[1] Kwak J. T., Xu S., and Wood B. J. (2015), "Efficient data mining for local binary pattern in texture image analysis," *Expert Syst. Appl.*, Vol. 42, No. 9, pp. 4529–4539.
[2] Dan Z., Chen Y., Yang Z., and Wu G. (2014), "An improved local binary pattern for texture classification," *Opt. - Int. J. Light Electron Opt.*, Vol. 125, No. 20, pp. 6320–6324.
[3] Guo Z., Zhang L., and Zhang D. (2010), "A Completed Modeling of Local Binary Pattern Operator for Texture Classification," *IEEE Trans. Image Process.*, Vol. 16, No. 6, pp. 1657–1663.
[4] Liu L., Zhao L., Long L., Kuang G., and Fieguth P. (2012), "Extended local binary patterns for texture classification," *Image Vis. Comput.*, Vol. 30, No. 2, pp. 86–99.
[5] Ojala T., Pietikäinen M., and Mäenpää T.(2002), "Multiresolution gray-scale and rotation invariant texture classification with local binary patterns,"*TPAMI*, vol. 24, no. 7, pp. 971–987.
[6] Guo Z., Li Q., You J., Zhang D., and Liu W.(2012), "Local directional derivative pattern for rotation invariant texture classification," *Neural Comput. Appl.*, vol. 21, no. 8, pp. 1893–1904.
[7] Ahonen T.(2009), "Rotation Invariant Image Description with Local," *Scia*, pp. 61–70.

[8] Varma M. and Zisserman A. (2009), “A statistical approach to material classification using image patch exemplars,” *IEEE Trans. Pattern Anal. Mach. Intell.*, vol. 31, no. 11, pp. 2032–2047.
[9] Xu Y., Yang X., Ling H., and Ji H.(2018), “A new texture descriptor using multifractal analysis in multi-orientation wavelet pyramid,” *Proc. IEEE Comput. Soc. Conf.*, no. 60603022, pp. 161–168, 2018.
[10] Heikkilä M., Pietikäinen M., and Heikkilä J.(2014), “A texture-based method for detecting moving objects.,” *Bmvc*, Vol. 28, No. 4, pp. 21.1–21.10.
[11] Baravalle J. C. G., Rodrigo Guillermo, Claudio Delrieux (2015), “Multifractal characterisation and classification of bread crumb digital images,” vol. 9, pp. 1–10.
[12] Zhao G. and Ahonen T.(2017), “Rotation Invariant Image and Video Description with Local Binary Pattern Features,” *IEEE Trans. Image Process.*, vol. 21, no. 4, pp. 1–13.
[13] Nanni L., Brahnam S., and Lumini A. (2019), “Combining different local binary pattern variants to boost performance,” *Expert Syst. Appl.*, vol. 38, no. 5, pp. 6209–6216.
[14] Ojala T., Pietikäinen M., and Mäenpää T.(2016), “Gray Scale and Rotation Invariant Texture Classification with Local Binary Patterns,” *In Pract.*, vol. 1842, pp. 404–420.
[15] Shrivastava N. and Tyagi V. (2017), “An effective scheme for image texture classification based on binary local structure pattern,” *Springer-Verlag Berlin Heidelb.*, vol. 30, pp. 1223–1232.
[16] Zhao G. and Matti P.(2017), “Local Binary Patterns with an Application to Facial Expressions,” *Pattern Anal. Mach. Intell. Trans.*, vol. 29, no. 6, pp. 915–928.
[17] Sørensen L., Shaker S.B., and De Bruijne M. (2019), “Quantitative Analysis of Pulmonary Emphysema using Local Binary Patterns,” *IEEE Trans. Med. Imaging*, vol. 29, no. 2, pp. 559–569.
[18] Hemsley A. and Mukundan R.(2009), “Multifractal Measures for Tissue Image Classification and Retrieval,” *2009 11th IEEE Int. Symp. Multimed.*, pp. 618–623.
[19] Mukundan R. and Hemsley A.(2010), “Tissue Image Classification Using Multi-Fractal Spectra,” *Int. J. Multimed. Data Eng. Manag.*, Vol. 1, No. 2, pp. 62–75, Jan.
[20] Ibrahim M. and Mukundan R.(2014), “Multi-fractal Techniques for Emphysema Classification in Lung Tissue Images,” *Int. Proc. Chem. Environ. Eng.*, vol. 78, pp. 115–119.
[21] Zhang H.(2009), “A Novel Bayes Model: Hidden Naive Bayes,” *IEEE Trans. Knowl. Data Eng.*, Vol. 21, No. 10,
[22] Mikolajczyk K. and Schmid C.(2015), “Performance evaluation of local descriptors.,” *IEEE Trans. Pattern Anal. Mach. Intell.*, vol. 27, no. 10, pp. 1615–30.
[23] Ibrahim M.A. and Mukundan R.(2016), “Cascaded techniques for improving emphysema classification in computed tomography images,” *Artif. Intell. Res.*, vol. 4, no. 2, pp. 112–118.
[24] Demšar J. (2006), “Statistical Comparisons of Classifiers over Multiple Data Sets,” *J. Mach. L Res.*,Vol. 7.
[25] Breiman L.(2001), “Random forests,” *Mach. Learn.*, Vol. 45, pp. 5–32.
[26] Wang L.(2015), *Support Vector Machines : Theory and Applications*. Berlin: Springer-Verlag.
[27] Mitra V., Wang C.J., and Banerjee S.(2016), “Lidar detection of underwater objects using a neuro-SVM-based architecture,” *IEEE Trans. Neural Networks*, vol. 17, no. 3, pp. 717–731.
[28] Fu X. and Wang X.(2003), “Data dimensionality reduction with application to simplifying RBF network structure and improving classification performance,” *IEEE Trans. Syst. Man, Cybern. Part B Cybern.*, vol. 33, No. 3, pp. 399–409.
[29] Zhang L., Wang L., and Lin W.(2011), “Biased subspace learning for SVM Relevance Feedback in Content-Based Image Retrieval,” *ICICS 2011 - 8th Int. Conf. Information, Commun. Signal Process*.
[30] Zhang L., Sember S., Wang L. and Lin W.(2012), “Information for Collaborative Image Retrieval,” *IEEE Trans. Image Process.*, vol. 21, No. 8, pp. 3707–3720.